Acta Cryst. (1997). D53, 691–702

Lysozyme Aggregation Studied by Light Scattering. I. Influence of Concentration and Nature of Electrolytes

YANNIS GEORGALIS,* PATRICK UMBACH, JANNIS RAPTIS AND WOLFRAM SAENGER

Institut für Kristallographie, Freie Universität Berlin, Takustrasse 6, Germany. E-mail: yannis@chemie.fu-berlin.de

(Received 30 December 1996; accepted 6 May 1997)

Abstract

Static and dynamic light scattering have been employed to investigate the behaviour of lysozyme solutions when varying the concentration of $(NH_4)_2SO_4$ and NaCl for screening the repulsive forces between the monomers. At the initial aggregation stages clusters, which can be classified as mass-fractals undergoing diffusion limited-like aggregation, coexist with monomers or small lysozyme oligomers. The kinetics of fractal growth deliver observables that exhibit distinct tendencies when examined as a function of the concentration and nature of the electrolyte. The behaviour of the observables changes drastically above $0.84\,M$ $(NH_4)_2SO_4$ and $0.60\,M$ NaCl. Static light scattering revealed a progressive restructuring of the fractals to compact structures at the latter stages of the reaction. Based on the correlations between the various observables an attempt is made to predict the long-term fate of the nucleating solutions.

1. Introduction

The search for optimal crystallization conditions is an important aspect for obtaining protein crystals suitable for X-ray analysis. The relative lack of kinetic data and non-systematic screening of crystallization attempts has so far prohibited the development of adequate protein crystallization diagnostics. We have, therefore, focused on the study of lysozyme for observing the events involved in nucleation and concomitant microstructure formation. The crystallization of lysozyme, employing NaCl and $(NH_4)_2SO_4$ as screening electrolytes, has been explored by Kam, Shore & Feher (1978); Feher & Kam (1985) by us (Georgalis & Saenger, 1993; Georgalis, Zouni, Eberstein & Saenger, 1993; Georgalis, Schüler, Eberstein & Saenger, 1994; Georgalis, Schüler, Frank, Soumpasis & Saenger, 1995; Eberstein, Georgalis & Saenger, 1994) and other investigators (see references in Ducruix & Giegé, 1992, Niimura, Minezaki, Ataka & Katsura, 1995; Muschol & Rosenberger, 1995) using light and small-angle neutron scattering techniques. The aspects concerning protein crystallization have recently been reviewed by Giegé, Drenth, Ducruix, McPherson & Saenger (1995) in a paper involving 291 citations.

Two limiting regimes are thought to adequately represent the kinetics of aggregating systems. The first is termed diffusion-limited (DLCA) and the second reaction-limited (RLCA) cluster–cluster aggregation (van Dongen & Ernst, 1985*a*,*b*; Lin *et al.*, 1989*a*,*b*). DLCA is characterized by power-law growth kinetics and a universal fractal dimension of 1.81, whereas RLCA by exponential growth kinetics and a universal fraction dimension of 2.1 (Klein *et al.*, 1990). The fractal dimension depends also on the kind of collision *i.e.* monomer–cluster or cluster–cluster and on restructuring, a property difficult to capture experimentally. Therefore, the identification of aggregation regimes may not always be unambiguous (Vicsek, 1989).

The sticking probability on impact, α, defines the onset of each aggregation regime (*cf.* equation 1). The value of α is theoretically equal to unity for DLCA and zero for RLCA type of kinetics. One should be aware that this definition reflects only ideal limiting situations. The theory of aggregation, as developed by Smoluchowski (1916*a*,*b*, 1917), neglects the development of repulsive barriers between particles and presumes aggregates formed only by attachment of seeding particles to a preexisting cluster, ignoring cluster–cluster collisions. This theory was further developed by introducing a potential that reduces the aggregation rates by a factor known as the sticking probability, α, which can be approximated by known expressions at low electrolyte and monomer concentrations (Sonntag & Strenge, 1987). For concentrated systems, the exact interpretation of the sticking probability becomes increasingly difficult, unless defined in the frame of an effective interaction potential (see *Discussion* section).

Light scattering is a suitable method for investigating changes in aggregation behaviour. For non-stationary nucleating solutions, the events can be examined by time-resolved dynamic light scattering (DLS) which provides information on the particle size distribution through measurement of the autocorrelation function (ACF) of the scattered light which is associated with the diffusion coefficient and hydrodynamic radius of the particles. The technique has been reviewed by Schmitz

(1990); Chu (1991) and more recently by Brown (1993).

The DLS spectra of nucleating lysozyme solutions are dominated by mass-fractals whose treatment is associated with some difficulties: (i) the examined nucleating solutions depart from the dilute regime, as the cluster-size distribution involves species spanning more than three orders of magnitude in radius space; (ii) particle radii increase rapidly to sizes comparable to the wavelength of light thus resulting in substantial interparticle interferences; (iii) the ACF of the scattered light is a superposition of exponentials characterized by a distribution of relaxation times and scattering amplitudes proportional to the light scattered by each species. The resolution of a sum of exponentials is known to comprise an ill-conditioned problem (Provencher, 1982*a*,*b*) and renders data analysis difficult; (vi) since mass-fractals are asymmetric structures, the contributions of rotational diffusive modes should be decoupled from the translational modes. All these deviations from standard DLS in dilute stationary solutions pose severe restrictions in the experimental design, data acquisition and concomitant evaluation procedures. Complex, although tractable, is the formulation of the ACF involving an integration over the cluster size distribution; corrections for the contribution of the rotational modes have been given by Lindsay, Klein, Weitz, Lin & Meakin (1988, 1989) and were further elaborated by Lin *et al.* (1989*a*,*b*).

In time-resolved DLS experiments we can decouple at least two predominant particle populations, the first representing lysozyme monomers (or oligomers) and the second mass-fractal clusters (Meakin, 1988). The evaluation of the spectra allows for the determination of the radius of the small oligomeric species with radius R_m. The latter corresponds to the stationary component that appears in the correlograms. It is determined as an average over all spectra in a kinetic experiment. If their scattering amplitudes allow, their mean radius can be precisely determined. In a previous work (Eberstein *et al.*, 1994), it was shown that crucial parameters, like the charge of the monomeric lysozyme and a 0.50 *M* NaCl concentration for triggering aggregation can be deduced from the concentration dependence of the diffusion coefficient of the small oligomers, after decoupling the contribution of the fractal aggregates. Further, the observables deduced from the growth kinetics are: (i) the fractal dimension of the cluster, d_f; (ii) the zero-time extrapolated cluster radius, $R_H(0)$; (iii) the 'quasi-stationary' hydrodynamic radius, R_h^{qs}, taken as an average radius of all records between 30 and 35 min (*i.e.* when the kinetics have levelled off) and (iv) tentative estimates of the sticking probability, α, that typifies the aggregation process. When the fractals exceed μm sizes, DLS ceases to deliver meaningful information and static light scattering (SLS) is employed to investigate the average cluster morphology.

In this work we have examined the aggregation of lysozyme induced by NaCl and $(NH_4)_2SO_4$ for screening the repulsive electrostatic forces acting on lysozyme molecules. The concentration of lysozyme was kept constant (1.03 m*M*) and was chosen to render the crystallization conditions suboptimal. The task is to find the coupling between the various observables and to draw conclusions concerning the long-term fate of the nucleating solutions.

2. Materials and methods

The chemicals used in the present work were of analytical grade. Three times crystallized lysozyme purchased from Sigma Chemical Co. (Deisenhofen, Germany) was dialyzed against water to remove excess NaCl (100 m*M* by osmometry) and lyophilized. All experiments were conducted in a buffer containing 0.1 *M* Na acetate pH 4.25 $(NH_4)_2SO_4$ and NaCl p.a. grade, were from Merck (Darmstadt, Germany).
Sodium dodecyl sulfate polyacrylamide gel electrophoresis (SDS–PAGE) of lysozyme revealed a major 14.5 kDa and a minor, *ca* 1% at 3.4 kDa, band with overloaded silver-stained gels. Monodispersity of the preparations was controlled by DLS before the kinetic experiments, without added electrolyte. For aggregation experiments lysozyme and electrolyte were rapidly mixed in the appropriate ratio and filtered through Minisart sterile filters, 0.2 μm pore size, into standard cylindrical light scattering cells. DLS monitoring was initiated within 30 s after mixing.

DLS measurements were conducted with an ALV/SP-86 spectrogoniometer (ALV, Langen, Germany) and the ALV-FAST/5000E digital autocorrelator boards at a scattering angle of 20°. An Ar^+ Spectraphysics 2017 laser (operating wavelength 488 nm, maximal output power 2.0 W in TEM_{00} mode) served as light source. All experiments were conducted at a constant temperature, 293 ± 1 K, and spectra were collected every 30 s for 35 min. The total number of counts collected per spectrum was well above the threshold of 1×10^7 counts required for successful Laplace inversions with a modified version of the program *CONTIN* (Provencher, 1982*a*,*b*). Laplace inversions were computed in a 45-point logarithmic quadrature grid imposing non-negativity constraints. Solution viscosities and refractive indices of water as a function of $(NH_4)_2SO_4$ and NaCl concentration were obtained from standard tables (Handbook of Chemistry and Physics, 1984–1985).

SLS measurements were performed in the same spectrogoniometer at angles between 15 and 110° corresponding to scattering vectors of 4.50×10^{-3} and 2.81×10^{-2} nm^{-1}, respectively. Intensities were collected with a resolution of 2.5° and the duration of each

angular scan was 40 min. A second ALV/SO-SIPD fiber-optic detection unit was installed at a scattering angle of 270°. The scattered intensities collected with this detector were evaluated separately. A fraction of the laser beam was monitored by two quadrant photodiodes placed behind and after a precision attenuator (Newport, USA). The intensity values from the photodiodes were employed for normalizing each data set, and to exclude artefacts stemming from long-term fluctuations and changes in the pointing stability of the laser beam.

3. Results and discussion

Aggregation kinetics were studied at an intermediate lysozyme concentration, 1.03 m*M*. There is a good reason for this choice. We know *a priori* (see below) that this lysozyme concentration renders crystallization conditions suboptimal and we want to examine the effects introduced by changing the electrolyte concentration.

The concentration of $(NH_4)_2SO_4$ was varied between 0.10 and 1.40 *M* and that of NaCl between 0.30 and 0.80 *M*. Crystals were not observed at all when aggregation was induced by $(NH_4)_2SO_4$. Solubility and power spectroscopy studies (Kam *et al.*, 1978; Riès-Kautt & Ducruix, 1989) have shown that $(NH_4)_2SO_4$ does not promote the crystallization of lysozyme at pH 4.25. Crystallization of lysozyme using $(NH_4)_2SO_4$ was reported at nine- to 14-fold higher lysozyme concentrations, using specially purified (isoionic) lysozyme at pH ranging between 8 and 9 (Riès-Kautt, Ducruix & Dorsselaer, 1994). Such high protein concentrations resemble closely those established in phase separation studies (Ishimoto & Tanaka, 1977; Thomson, Schurtenberger, Thurston & Benedek, 1987; Taratuta, Holschbach, Thurston, Blankschtein & Benedek, 1990). The optimum concentration for crystallization of lysozyme with NaCl was found between 0.50 and 0.70 *M* (Eberstein *et al.*, 1994; Georgalis *et al.*, 1995); large crystals appear within 2 d with 1.55 m*M* lysozyme. Longer times, 6–12 d, are required for observing microcrystals with 1.03 m*M* lysozyme at 0.80 *M* NaCl.

A typical time-resolved DLS experiment involving 1.03 m*M* lysozyme and 0.70 *M* NaCl is depicted in Fig. 1. It involves selected ACF's plotted as a function delay time and the respective distributions of mean hydrodynamic radii. The smaller component in the distributions corresponds to monomeric (or oligomeric) lysozyme; its radius remains stable throughout whereas its amplitude is reduced. The later component resembles mass-fractal clusters; both their amplitudes and mean cluster radii evolve with reaction time.

The mean hydrodynamic radius of the small oligomers, R_m, is determined as an average over all spectra in a series of kinetic experiments. The lysozyme monomer radius is 1.96 nm and corresponds to a diffusion coefficient of 11×10^{-7} cm^2 s^{-1} (Dubin, Noel & Benedek, 1971). A rough estimate of the lysozyme dimer radius, 2.73 nm, can be obtained from the dimer-to-monomer ratio of the diffusion coefficients of hard spheres (Batchelor, 1976), which is 0.719.

R_m increases linearly with increasing $(NH_4)_2SO_4$ concentration. Stable dimers are expected to form at around 1.50 *M* $(NH_4)_2SO_4$, Fig. 2(*a*). If aggregation is induced by NaCl, R_m deviates reproducibly from linearity below 0.50 *M* most probably because of structural changes and interactions (the two points at 0.3 and 0.4 *M* were omitted from the linear fit), Fig. 2(*b*). Above this concentration, R_m increases, but again it does not attain the radius expected for stable dimers. For $(NH_4)_2SO_4$ the coefficients of the linear fit are: $b_0 = (1.95 \pm 0.12)$ and $b_1 = (5.37 \pm 0.03) \times 10^{-1}$ and

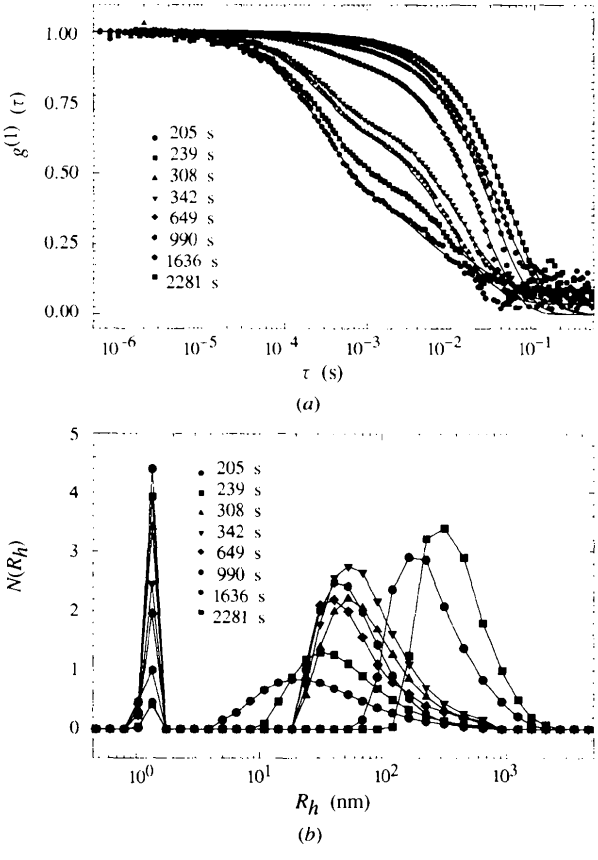

Fig. 1. Typical time-resolved DLS experiment with 1.03 m*M* lysozyme and 0.70 *M* NaCl in 0.1 *M* Na acetate buffer, pH 4.25 at 293 K peformed at a scattering angle of 20°. (*a*) Selected first-order autocorrelation functions, $g^{(1)}(\tau)$, plotted as a function of delay time τ. (*b*) The respective hydrodynamic radii distributions, $N(R_h)$, deduced by *CONTIN*. The radius of the smallest component corresponds to monomeric (or oligomeric) lysozyme; it remains constant throughout whereas its amplitude is reduced. The larger component resembles mass-fractal clusters; both amplitude and mean radius evolve with time.

for NaCl $b_0 = (1.92 \pm 0.03)$ and $b_1 = (2.7 \pm 0.04) \times 10^{-1}$. R_m extrapolates close to the radius of the lysozyme monomer, 1.96 nm, for both electrolytes. The formation of stable dimers is the rate-limiting step for any further aggregation. If it is prohibited due to repulsion, the probability for nuclei to grow will be negligible. The increment of R_m with increasing electrolyte concentration can be attributed to the concentration dependence of the diffusion coefficient of lysozyme in the presence of screening electrolyte.* Since higher order aggregates are formed in the solutions, the behaviour of R_m does not imply complete absence of stable dimers but rather insufficient quantities for being successfully monitored by DLS. The observed R_m values are expected to reflect an average radius between the purely monomeric lysozyme and higher order aggregates. These two populations cannot be resolved by DLS. We can conclude that the chosen lysozyme concentration does not directly favour the formation of stable dimers in the examined electrolyte concentration range.

The hydrodynamic radius $R_h(t)$ of the $(NH_4)_2SO_4$ and NaCl fractals is plotted as a function of time in Fig. 3. The depicted experiments represent selected measurements from two to three repetitions. The deviations in the mean radii of the evolving lysozyme clusters were less than 15%. This accuracy is sufficient for providing reliable estimates of the various observables. The kinetic data were fitted with a power-law dependence

$$R_h(t) = R_h(0)(1 + \alpha c_s t)^{z/d_f}, \; c_s = \frac{4k_BT}{3\eta} N_0, \qquad (1)$$

where $R_h(0)$ denotes the zero-time extrapolated cluster radius, d_f the fractal dimension and α the sticking probability on collision. The dynamic exponent z describes the reactivity between clusters and is equal to unity for pure DLCA kinetics. c_s denotes the Smoluchowski (1916*a*,*b*, 1917) rate constant that typifies the kinetics, k_BT the thermal energy, η the viscosity of the solvent and N_0 the number of monomer

* A full treatment of this issue is beyond the scope of the present work; details can be found in Wills & Georgalis (1981); Pusey & Tough (1985); Eberstein *et al.* (1994) and Muschol & Rosenberger (1995).

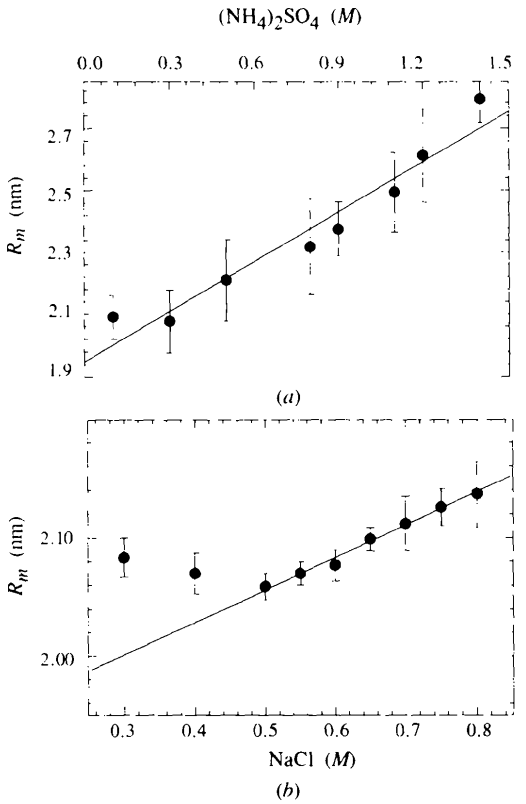

Fig. 2. Mean hydrodynamic radius R_m of the oligomeric lysozyme clusters as function the electrolyte concentration. (*a*) Stable dimers and larger oligomeric species are formed above 1.0 *M* $(NH_4)_2SO_4$. (*b*) If the aggregation kinetics are induced by NaCl, radii that could resemble those of stable dimers are not observed due to the low lysozyme concentation employed.

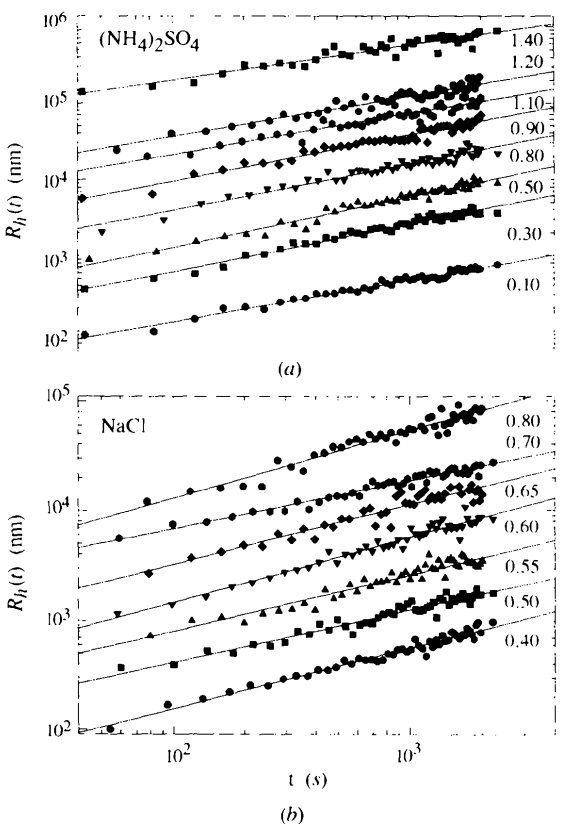

Fig. 3. Selected time-resolved kinetics of lysozyme. Mean hydrodynamic radii $R_h(t)$ of the formed clusters are plotted as a function of the reaction time t. The numbering at each curve denotes the concentrations of (*a*) $(NH_4)_2SO_4$ and (*b*) NaCl in *M*. Other conditions were as in the *Materials and methods* section. For the sake of clarity the curves are shifted from bottom to top by ascending powers of 2.

particles at time zero. RLCA-type fits were not justified by any of the data sets.

The observed kinetics corresponds to DLCA aggregation; although at the employed lysozyme volume fractions, gelation* should theoretically occur immediately (Sonntag & Strenge, 1987). The interplay between the exponents z and d_f could account for this behaviour. Asnaghi, Carpineti, Giglio & Sozzi (1992) have pointed out that fractal morphology may exhibit a quicker response to changes in the sticking probability than the kinetics *per se*. Some uncertainty is yet evident in the time-resolved DLS experiments if the dynamic exponent z (*cf.* equation 1) is assumed to be unity. While this assumption is often made when aggregation kinetics are explored by DLS, z can be unambiguously determined from the scaling of the weight-average mass on time using small-angle SLS. In a subsequent communication (Umbach, Georgalis & Saenger, 1997) we will show that z depends strongly on NaCl concentration and, at least at the later stages of the reaction, it deviates appreciably from unity. Consequently, we call this type of aggregation DLCA-like. Polarization effects, interactions between clusters and restructuring may account for the deviations from the theoretically expected aggregation times (Broide, 1988). Further, it should be stressed that biomolecules cannot be approximated as hard spheres and if anisotropy is taken into account, the correct positioning of monomers during the formation of lower order aggregates requires the consideration of an additional orientational probability (Northrup & Erickson, 1992).

When aggregation is induced by $(NH_4)_2SO_4$, the fractal dimension starts from typical DLCA values (Fig. 4*a*), goes through a minimum at 0.60 *M* and then rises to values larger than 2.00 around 1.4 *M* $(NH_4)_2SO_4$. The reduction of the fractal dimension to the minimum value of 1.5 is a consequence of the fact that clusters grow larger but also more tenuous, since most of collisions take place on their periphery. The increment of the fractal dimensions from the minimum to larger values than 2.00 signifies cluster percolation and the onset of a gelling transition. This had been verified by visual inspection of the light-scattering cells at high $(NH_4)_2SO_4$ concentrations after several days. When aggregation is induced by NaCl, the mean fractal dimension corresponds closely to 1.81 as expected for DLCA aggregation (Fig. 4*b*) if we do not attribute much significance in the fluctuations of d_f observed below 0.60 *M* NaCl. These small changes can be associated to structural changes involved in the seed particles building the fractals (see Figs. 2 and 5 and discussion below).

In previous work, using DLS and SAXS (small-angle X-ray scattering, Georgalis *et al.*, 1995), we have identified an intermediate population of stable clusters with radii resembling $R_h(0)$ (Fig. 5). For aggregation induced by $(NH_4)_2SO_4$, $R_h(0)$ remains nearly constant, around 10 nm, up to a concentration of 0.84 *M*, Fig. 5(*a*). Above this concentration it exhibits a smooth rise, up to 75 nm at 1.40 *M*. Cluster radii determined in aggregation induced by NaCl exhibit a clear minimum of 9 nm around 0.60 *M* NaCl, Fig. 5(*b*).

From the classical nucleation theory we expect that the radii of nuclei will increase until they reach their critical size (Wagner, 1961) which is not expected to drastically vary until crystallization is completed. The typical sigmoidal behaviour predicted by the theory (Dhont, Smits & Lekkerkerker, 1992) was observed by other investigators (Malkin, Cheung & McPherson, 1993; Malkin & McPherson, 1993*a*,*b*) during aggregation of viruses and proteins larger than lysozyme. For lysozyme DLS delivers radii between 10 and 35 nm for $R_h(0)$ whereas SAXS (Georgalis *et al.*, 1995) and a

* A gel can be understood as a large fractal which grows until it fills the whole volume (van Dongen & Ernst, 1985*a*,*b*).

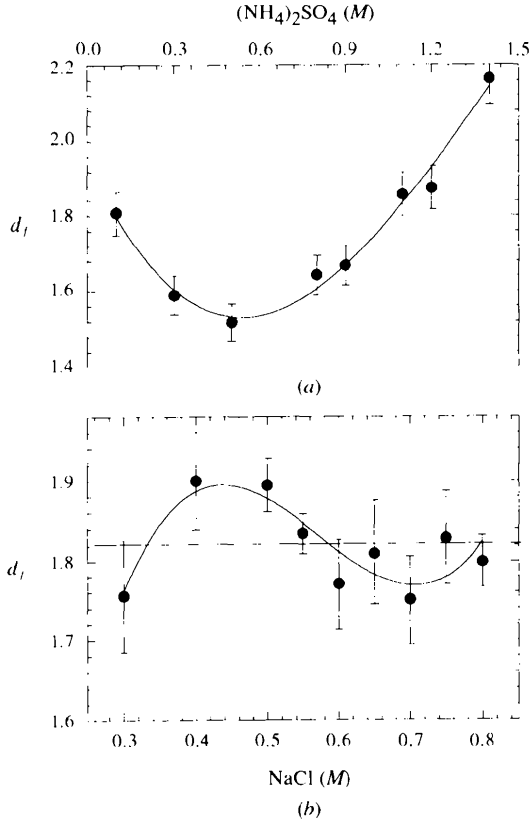

Fig. 4. Fractal dimension, d_f, of lysozyme clusters plotted as function of (*a*) NaCl and (*b*) $(NH_4)_2SO_4$ concentration. When aggregation is induced by $(NH_4)_2SO_4$ a pronounced minimum is observed. The further rise of d_f above 0.60 *M* signifies the evolution of percolated structures and the system is driven towards gel formation. In contrast to this behaviour, the fractal dimension of clusters remains constant around 1.82, characteristic of DLCA-like aggregation (see text for details) when aggregation is induced by NaCl. The curves through the points serve as guides to the eye.

recent small-angle neutron scattering (SANS) study (Niimura *et al.*, 1995) have shown that the radii of clusters prevailing in nucleating lysozyme solutions vary between 5 and 35 nm, depending on conditions. Whether these clusters are always identical, *i.e.* produced by the same aggregation mechanism, is not clear. It should be kept in mind that DLS, SAXS and SANS probe different spatial scales, and accounting for solution polydispersity is more difficult with SAXS and SANS than with DLS. Considering all these shortcomings, it is at least satisfactory that for comparable conditions, these cluster radii fall to within one order of magnitude.

For deducing tentative estimates of the cluster size within a series of time-resolved experiments, we have averaged the radii determined between 30 and 35 min after initiating the experiments and name it as 'quasi-stationary' radius, R_h^{qs}. Since the system is always far from stationary, fractals are expected to grow until they occupy the whole volume available and form gels, but this approximation is justified when growth levels off. Clear differences can be ascertained when comparing the quasi-stationary radii R_h^{qs} of the clusters in each electrolyte. When aggregation is induced by $(NH_4)_2SO_4$, Fig. 6(*a*), the radii grow in a monotonic fashion and reach values of *ca.* 1.45 μm above 0.84 *M* electrolyte. In contrast, when aggregation is induced by NaCl, Fig. 6(*b*), the radii exhibit a clear maximum of approximately 0.9 μm around 0.60 *M* NaCl and then drop again to lower values.*

Approximate estimates of the sticking probability α as a function of electrolyte concentration can be obtained using the values of R_h^{qs}, $R_h(0)$ and d_f determined from the time-resolved experiments (*cf.* equation 1). If aggregation is induced by $(NH_4)_2SO_4$, the values of α remain practically unchanged, around 0.23, up to 0.84 *M* and then drop in a monotonic fashion, Fig. 7(*a*). They are throughout lower than unity, which is by definition the expected value for DLCA aggregation. In contrast, if aggregating is induced by NaCl, α exhibits a clear maximum of 0.60

* The relative R_h^{qs} values are lower than previously reported (Georgalis *et al.*, 1995) due to the shorter duration of the kinetics.

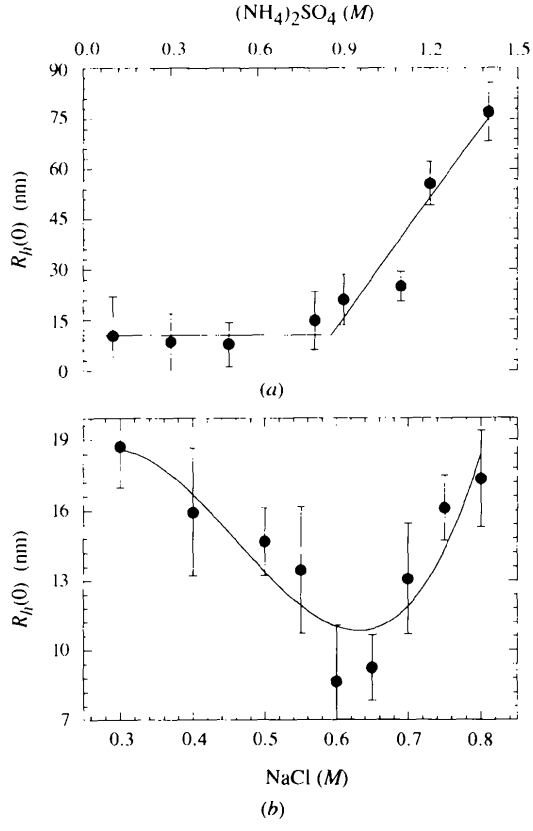

Fig. 5. Zero-time extrapolated cluster radius $R_h(0)$ as a function of electrolyte concentration. (*a*) A clear trend to larger radii becomes noticeable above 0.84 *M* $(NH_4)_2SO_4$. (*b*) If aggregation is induced by NaCl, a minimum with $R_h(0)$ of some 8 to 10 nm at 0.60 *M* is observed. The curves through the points serve a guides to the eye.

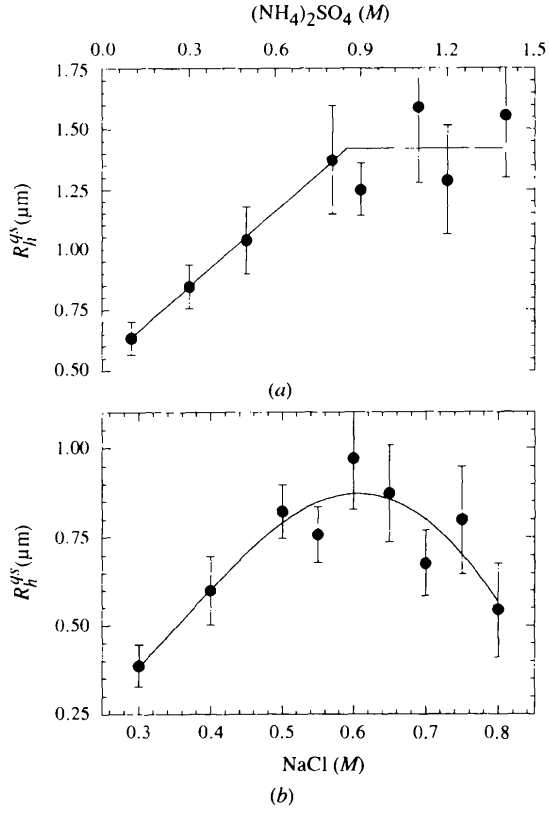

Fig. 6. Quasi-stationary radius, R_h^{qs}, as a function of electrolyte concentration. (*a*) An increment of R_h^{qs} up to a plateau around 1.5 μm is observed in aggregation induced above 0.84 *M* $(NH_4)_2SO_4$. (*b*) In NaCl induced aggregation, R_h^{qs} exhibits a maximum of 0.9 *M* around 0.60 *M* (see text for details). The curves through the points serve as guides to the eye.

at 0.58 *M* NaCl. Below and above this concentration, α drops to smaller values, Fig. 7(*b*). Whereas straightforward explanations for the observed behaviour of α are difficult, a qualitative discussion for the lysozyme–NaCl system is given in the next section. It should be noted that we cannot use α directly to explain the interconnection between other observables since it is a deduced variable. However, if some knowledge on the overall effective interactions is available, it can be correlated with the behaviour of α. Factors like binding of Cl^- ions to lysozyme could also affect the relative trends of the observables. Between 0.3 and 0.6 *M* NaCl 21–23 Cl^- ions bind to lysozyme, whereas only eight bind at 0.8 *M* NaCl, (Sibille & Pusey, 1994).

Selected SLS results are displayed in Fig. 8. Because of limited space only two distinct concentrations are considered for each electrolyte. Whereas SLS can provide very useful information for interacting solutions, here we are interested only on the morphology of the clusters. When the clusters enter the power-law regime (Schaefer, Bunker & Wicoxon, 1989) there is a simple relation connecting the scattered intensity with the fractal dimension, d_f,

$$\langle I(q)\rangle \propto q^{-d_f} \quad \text{if} \quad qR_g \gg 1, \tag{2}$$

where q denotes the scattering vector,

$$q = \frac{4\pi n}{\lambda} \sin\left(\frac{\theta}{2}\right), \tag{3}$$

that depends on the index of refraction of the medium, n, on the wavelength, λ, and on the scattering angle θ. R_g denotes the cluster radius of gyration. The latter can be determined from Fisher–Burford (Fisher & Burford, 1967) fits to the scattered intensity distributions. However, such an approach due to our high aggregation rates requires a closer proximity to low scattering angles than that attained by SLS. Within the range of examined scattering vectors, the experiments with $(NH_4)_2SO_4$ indicate a rather slow approach to the power-law regime, Figs. 8(*a*) and 8(*b*). In contrast, a clear power-law regime is attained if aggregation is induced by NaCl, Figs, 8(*c*) and 8(*d*).*

The fractal dimension of the clusters can be determined by linear regression in selected segments of the data in the high-q region. It is difficult to ascertain d_f when aggregation is induced by $(NH_4)_2SO_4$, but the NaCl data exhibit a clear power-law decay and d_f can be determined with confidence. For the first hour of aggregation (the total duration of each angular scan was 40 min), the dimensionalities of the NaCl clusters are compatible to those obtained by time-resolved DLS, *i.e.* close to 1.81. They increase with time and relax close to values typifying compact species within some 3 h (the solid lines in Figs. 8(*a*) and 8(*b*) indicate compact clusters with $d_f = 3.0$). The change of the fractal dimension with time may have its origin either in the formation of compact clusters through restructuring, and/or to parallel growth of compact structures *via* coalescance (*i.e.* nucleation).

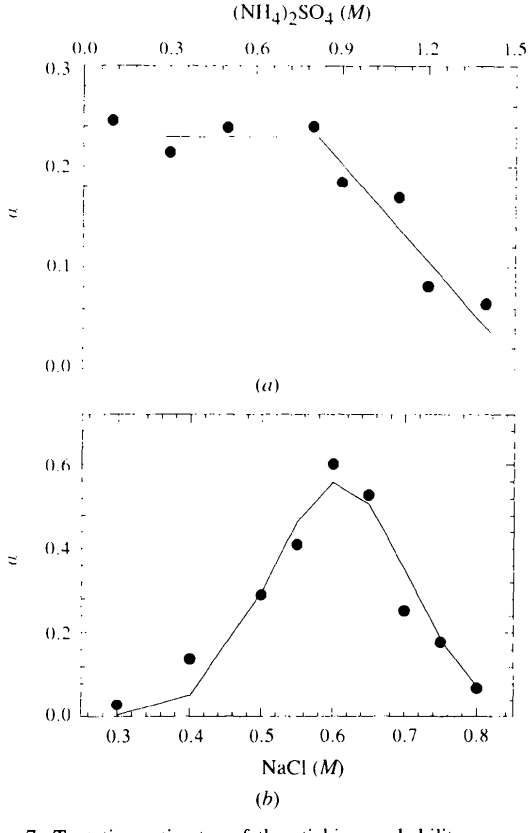

Fig. 7. Tentative estimates of the sticking probability, α computed from equation (1), plotted as a function of electrolyte concentration. If aggregation is induced by $(NH_4)_2SO_4$ the values of α remain initially unchanged around 0.23 up to a concentration of 0.84 *M* and then drop in a monotonic fashion. The estimates of α are throughout lower than unity expected for DLCA aggregation. In contrast, if aggregation is induced by NaCl, α exhibits a maximum value of 0.60 at 0.58 *M*. The curves through the points serve as guides to the eye.

4. Optical microscopy of lysozyme fractals

We have examined the formation of lysozyme fractals with high-resolution light microscopy at 1.1 *M* $(NH_4)_2SO_4$ and 0.7 *M* NaCl. The lysozyme concentration was in these experiments increased to 3.49 m*M* for easing observation. Typical tenuous and self-similar fractals with sizes of several μm grew between 3 and 30 h, Fig. 9. Their average morphology resembles those of DLCA fractals known form studies on colloids (Lin *et al.*, 1989*a*). After 30 h the intercluster distance is less

* A direct comparison between the fractal dimensions observed by time-resolved DLS and SLS is not possible since DLS corresponds to an 'isolated' fractal species whereas SLS involves weighted contributions from species.

than the average cluster dimension suggesting the onset of the gelling transition for both electrolytes.*

5. Interconnection between the observables

Since interconnection of the observed tendencies for R_m, $R_h(0)$ and R_h^{qs} is not trivial, we will limit ourselves in examining only very global features. R_h^{qs} and $R_h(0)$ are interconnected *via* the sticking probability of collision α (*cf.* equation 1) which depends on the effective cluster interactions. The theoretical behaviour of α is for both electrolyte systems, unknown. However, for the system lysozyme–NaCl we can still make reasonable guesses on the behaviour of α based on recent computations of the effective interaction potential of mean force (PMF) between monomers (Soumpasis & Georgalis, 1997). This potential is not monotonic and the interplay between packing and electrostatics cannot be expressed in simple terms. The computations of the PMF for the system lysozyme–NaCl have shown that the effective interactions lead to appreciable aggregation (which is necessary for crystallization) only in a narrow 'window' of electrolyte and protein concentrations. This is due to a solvent-mediated repulsive barrier which increases with increasing NaCl concentration. PMF computations for the lysozyme–$(NH_4)_2SO_4$ system are not yet available, although this electrolyte is very important for promoting protein crystallization. We expect again a complex behaviour of the PMF, since $(NH_4)_2SO_4$ is an asymmetric electrolyte that modifies strongly the water structure (Leberman & Soper, 1995).

To interpret the observed tendencies, we assume that clusters are built sequentially, in both electrolytes. Oligomers with radius R_m are formed immediately after the nucleation burst, and build larger seeds with radii

* Direct comparisons with the sizes deduced from the DLS experiments are difficult because of the different concentration employed and the two-dimensional character of the microscopic observation. The specimens are fixed by their own weight and do not undergo Brownian motion.

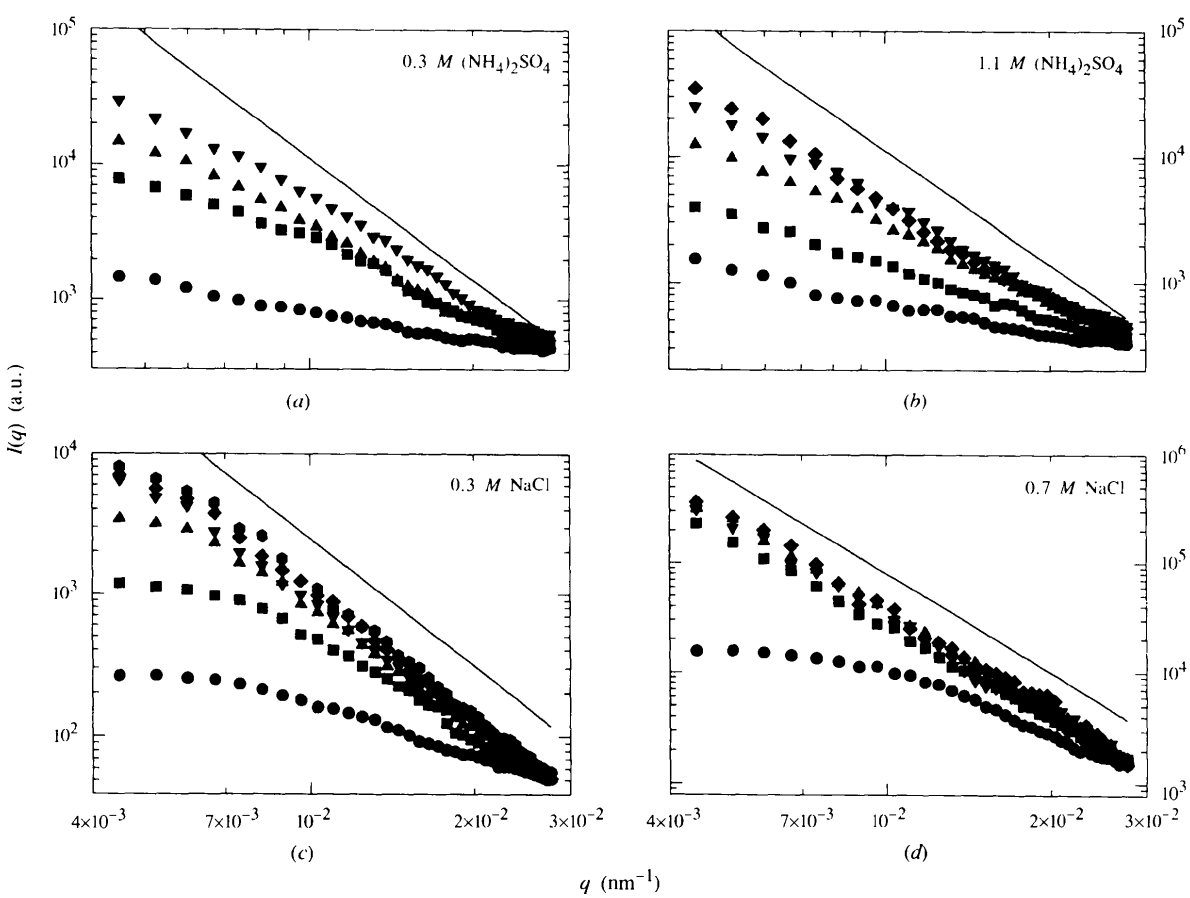

Fig. 8. Normalized SLS scattered intensities plotted as a function of scattering vector, q. The concentration of $(NH_4)_2SO_4$ was (*a*) 0.30 *M* and (*b*) 1.10 *M* and of NaCl (*c*) 0.30 *M* and (*d*) 0.70 *M*. Other conditions were as in the *Materials and methods* section. Note the progressive increase of the slopes as a function of time (symbols typify angular scans of *ca* 40 min). The observed behaviour can be understood either as restructuring of the fractal clusters and/or as evolution of compact species (nuclei). The solid line on each record which corresonds to $d_f = 3.0$ (*cf.* equation 2).

$R_h(0)$ which in turn form fractals typified by radii R_h^{qs}, at equivalent reaction times.

So far correlations between the observables for the system lysozyme–$(NH_4)_2SO_4$ have not been established. To understand the interconnection between $R_h(0)$ and R_h^{qs} as indicated by the discontinuities in Figs. 5(*a*), 6(*a*) and 7(*a*), we assume that around 0.84 *M* $(NH_4)_2SO_4$, changes occur in the system. Initially, small clusters with radius $R_h(0)$ aggregate to form larger fractals that reach a plateau radius for R_h above 0.84 *M* $(NH_4)_2SO_4$, Fig. 6(*a*). The trend of d_f (Fig. 4*a*), indicates that the fractals are increasingly more compact above 0.84 *M* $(NH_4)_2SO_4$. Therefore, the growth of constant size fractals from larger seeds (Figs. 5*a* and 6*a*) can be compensated by an increment of d_f and/or a reduction of α, Fig. 7(*a*). Improved screening is expected to render larger α values, and larger fractals to form at equivalent times. Since the seeds, with size $R_h(0)$, exhibit a constant radius below 0.86 *M* we are expecting an efficient balance between electrostatics and packing below 0.84 *M* $(NH_4)_2SO_4$. Above this concentration, repulsion dominates and α is gradually reduced. Both observables are then expected to exhibit counterbalancing tendencies (compare Fig. 5*a* with 7*a*). The changes in the system occurring around 0.84 *M* should be considered only qualitatively since no predictive models for the effective interactions are available. The data indicate the existence of an appreciable repulsive barrier around 0.80 *M* $(NH_4)_2SO_4$, but a persuasive proof, similar to that given for the lysozyme–NaCl system (Soumpasis & Georgalis, 1997), has not yet been performed.

Correlations between R_h^{qs} and $R_h(0)$ for the lysozyme–NaCl system, were shown to closely follow each other when plotted as a function of the protein and electrolyte concentration; both exhibit maxima at around 1.55 m*M* lysozyme and above 0.50 *M* NaCl (Georgalis *et al.*, 1995). If R_h^{qs} and $R_h(0)$ are at the maximum, larger nuclei formed immediately after the burst; they are expected to form larger fractals at equivalent times, if we assume a constant sticking probability under these conditions. The behaviour of $R_h(0)$, Fig. 5(*b*), exhibits the same tendency as in our previous work, namely $R_h(0)$ is at minimum in the same region of variable space.

The interconnection between $R_h(0)$ and R_h^{qs} can be understood if we invoke a structural transition of the monomer below 0.60 *M* NaCl that is expected to be transmitted to clusters with radii $R_h(0)$ and force them to pass through a minimum at comparable electrolyte concentrations (compare with Fig. 5*b*). Now, since the fractal dimension of these clusters remain nearly constant, Fig. 4(*b*), one would expect that fractals, with radius R_h^{qs}, grown from these seeds, will be forced to pass through a minimum. Instead, these clusters reproducibly pass through a maximum at around 0.60 *M* NaCl, Fig. 5(*b*). This behaviour can be attributed to changes in aggregation caused by the sticking probability, α, which is modified by the presence of NaCl as follows. Improved screening is expected to

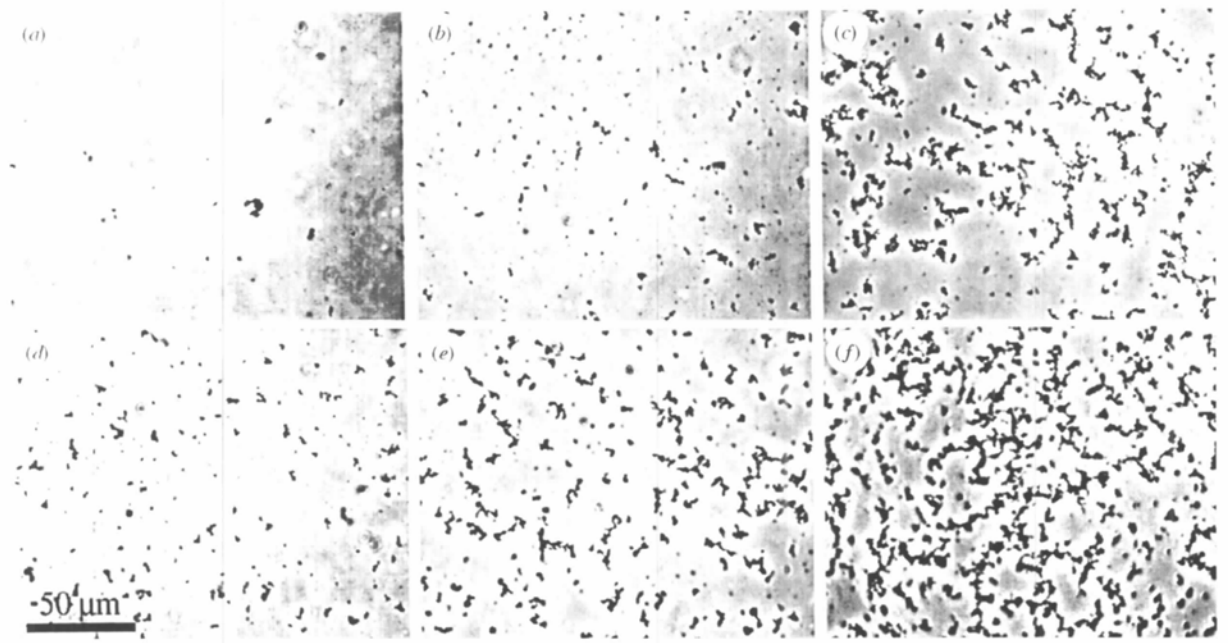

Fig. 9. Microscope images of lysozyme fractals. Lysozyme, 3.49 m*M*, was incubated with 1.1 *M* $(NH_4)_2SO_4$ (*a*, *b*, *c*) and 0.70 *M* NaCl (*d*, *e*, *f*). Other conditions as in *Materials and methods*. Images were recorded in (*a*, *d*) after 3 h, in (*b*, *e*) after 18 h and (*c*, *f*) after 30 h with an inverted Axiovert-100 microscope (Zeiss-Germany) in 1.0 mm flat quartz cells. Aggregation was allowed to proceed without moving or repositioning the microscope cell, since any manipulation may drastically alter the characteristics of the fragile fractal clusters.

render the magnitude of sticking probability higher and larger fractals to form at equivalent times. The fact that they grow from smaller seeding particles is compensated by the larger increment of α around 0.6 M NaCl in comparison with the increment observed in $(NH_4)_2SO_4$. However, we have shown that NaCl induces repulsion at 0.60 M. Then the sticking probability will be reduced, and both observables will pass through a maximum at this electrolyte concentration (compare Figs. 6*b* and 7*b*).

These explanations are tentative albeit no unreasonable within the precision of the experiments and the predictions of the PMF of lysozyme–NaCl system. The interplay between packing and electrostatics, which cannot be described by the DLVO (Derjaguin–Landau–Verwey–Overbeek) theory (Hunter, 1991), will be important for predicting crystallization conditions and emphasizes the role of solvent-mediated interactions. For pursuing more quantitative studies, estimates of the concentration of the species participating in nucleating solutions will be required.

6. Concluding remarks

The use of time-resolved DLS and SLS allows for a first-order analysis of lysozyme nucleation and cluster growth formation. Several observables can be readily deduced during the first hour of aggregation using DLS, whereas the evolution of compact structure can be better captured by SLS at the later stages of the reaction. The results obtained show that the clusters are fractals that reach μm sizes within 35 min, and whose growth can be described by DLCA power-law kinetics. These clusters are formed by small aggregates with radii $R_h(0)$ varying between 5 and 75 nm for $(NH_4)_2SO_4$, and 9 and 18 nm for NaCl (Fig. 5).

The results indicated that some of the monomers transform into clusters immediately after the addition of electrolyte (nucleation burst). One is tempted to identify this populations with nuclei with an upper radius limit equal to $R_h(0)$. The effective volume fraction of colliding species and therefore, the aggregation rates will be reduced (*cf.* equation 1) immediately after this burst. Under unfavourable conditions, these clusters are consumed in building fractals and never attain sizes and quantities required for spontaneous fuelling of crystal formation. Because of the small size of lysozyme, capturing the nucleation burst with methods like time-resolved SLS and DLS is impossible because its frame may be much shorter than the dead time of our experiment. Different trends, depending on the nature and concentration of the electrolytes, are pronounced for all observables. This is a consequence of the different interaction patterns of the electrolytes with both solvent (water) and lysozyme.

For the lysozyme–NaCl system the behaviour of $R_h(0)$ and R_m implies that the crystallization conditions are sub-optimal. This has been also verified by microscopic observations. At the examined lysozyme concentration, microcrystals were observed above 0.80 M NaCl after 21 d. From the regression in Fig. 2(*b*) we can estimate that 2.85 M NaCl will be required

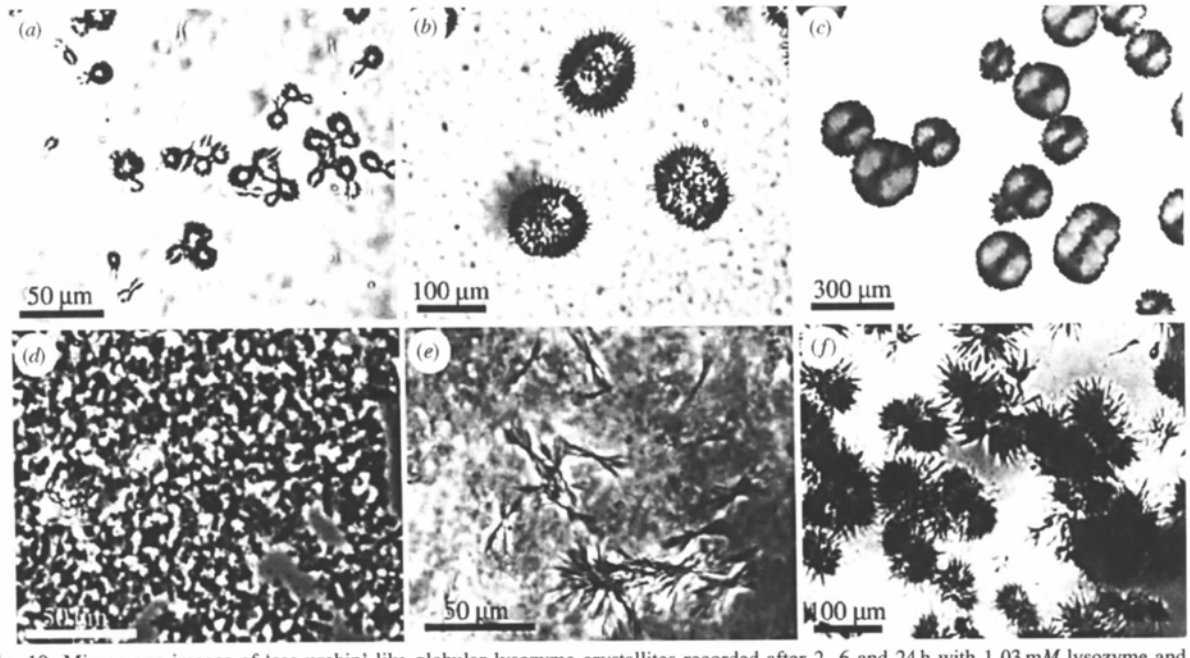

Fig. 10. Microscope images of 'sea-urchin' like globular lysozyme crystallites recorded after 2, 6 and 24 h with 1.03 mM lysozyme and 2.0 (*a*, *b*, *c*) or 2.85 M (*d*, *e*, *f*) NaCl. Other conditions as in *Materials and methods*. The electrolyte concentration was chosen from a prediction made using the linear dependence of R_m on NaCl concentration, (Fig. 2*b*).

to attain the radius of a stable dimer, with a radius 2.72 nm. Microscopic observations at 2.00 and 3.00 *M* NaCl showed that globular crystallites are formed within 6 h (Fig. 10) which are unsuitable for X-ray diffraction. Above 1.55 m*M* lysozyme and 0.70 *M* NaCl tetragonal crystals suitable for diffraction appear within 2 d. In summary, if lysozyme aggregation is induced by $(NH_4)_2SO_4$, a gelation transition is favoured more than crystal formation. If aggregation is induced by NaCl, the low lysozyme concentration chosen, will also preclude crystal formation.

The empirical correlations between the various observables and their extrema indicate that the information derived from the scattering experiments is useful for a first-order screening of crystallization conditions whereas estimates of the relative species involved in the nucleation reaction and predictions of the effective interactions are mandatory. Further experimental and theoretical extensions on these issues are under way.

This work was supported by grants from the Deutsche Forschungsgemeinschaft (Sa 196/26-1) to YG and by the DESY 05 641KEB project to PU.

References

Asnaghi, D., Carpineti, M., Giglio, M. & Sozzi, M. (1992). *Phys. Rev. A*, **45**(2), 1018–1023.

Batchelor, G. K. (1976). *J. Fluid Mech.* **74**, 1–29.

Broide, M. L. (1988). PhD thesis, Massachusetts Institute of Technology, USA.

Brown, W. (1993). *Dynamic Light Scattering, the Method and some Applications*. Oxford Science Publications.

Chu, B. (1991). *Dynamic Light Scattering*. New York: Academic Press.

Dhont, J. K. G., Smits, C. & Lekkerkerker, H. N. W. (1992). *J. Colloid Interface Sci.* **152**(2), 386–401.

van Dongen, P. G. J. & Ernst, M. H. (1985*a*). *J. Phys. A. Math. Gen.* **18**, 2779–2793.

van Dongen, P. G. J. & Ernst, M. H. (1985*b*). *Phys. Rev. Lett.* **13**, 1396–1399.

Dubin, S. B., Noel, A. C. & Benedek, G. B. (1971). *J. Chem. Phys.* **54**, 5158–5163.

Ducruix, A. F. & Giegé, R. (1992). *Crystalization of Nucleic Acids and Proteins*. Oxford: IRL Press.

Eberstein, W., Georgalis, Y. & Saenger, W. (1994). *J. Cryst. Growth*, **143**, 71–78.

Feher, G. & Kam, Z. (1985). *Methods Enzymol.* **114**, 77–112.

Fisher, M. E. & Burford, R. J. (1967). *Phys. Rev. A*, **156**(2), 583–622.

Georgalis, Y. & Saenger, W. (1993). *Adv. Colloid Interface Sci.* **46**, 165–183.

Georgalis, Y., Schüler, J., Eberstein, W. & Saenger, W. (1994). *Fractals in the Natural and Applied Sciences*, edited by M. M. Novak, pp. 139–151. North-Holland: Elsevier Science.

Georgalis, Y., Schüler, J., Frank, J., Soumpasis, D. M. & Saenger, W. (1995). *Adv. Colloid Interface Sci.* **58**, 57–86.

Georgalis, Y., Umbach, P., Raptis, J. & Saenger, W. (1997). *Acta Cryst.* D**53**, 703–712.

Georgalis, Y., Zouni, A, Eberstein, W. & Saenger, W. (1993). *J. Cryst. Growth*, **126**, 245–260.

Giegé, R., Drenth, J, Ducruix, A. F., McPherson, A. & Saenger, W. (1995). *Prog. Cryst. Growth Charact.* **30**, 237–281.

Handbook of Chemistry and Physics (1984–1985). Edited by R. C. Weast. Cleveland, Ohio, USA: The Chemical Rubber Co.

Hunter, R. J. (1991). *Foundations of Colloid Science*. Oxford Science Press.

Ishimoto, C. & Tanaka, T. (1977). *Phys. Rev. Lett.* **39**(8), 474–477.

Kam, Z., Shore, H. B. & Feher, G. (1978). *J. Mol. Biol.* **123**, 539–555.

Klein, R., Weitz, D. A., Lin, M. Y., Lindsay, H. M., Ball, R. C. & Meakin, P. (1990). *Prog. Colloid Polym. Sci.* **81**, 161–168.

Leberman, R. & Soper, K. A. (1995). *Nature (London)*, **378**(23), 364–366.

Lin, M. Y., Lindsay, H. M., Weitz, D. A., Ball, R. C., Klein, R. & Meakin, P. (1989*a*). *Nature (London)*, **339**, 360–362.

Lin, M. Y., Lindsay, H. M., Weitz, D. A., Ball, R. C., Klein, R. & Meakin, P. (1989*b*). *Proc. R. Soc. London Ser. A*, **423**, 71–87.

Lindsay, H. M., Klein, R., Weitz, D. A., Lin, M. Y. & Meakin, P. (1988). *Phys. Rev. A*, **38**(5), 2614–2626.

Lindsay, H. M., Klein, R., Weitz, D. A., Lin, M. Y. & Meakin, P. (1989). *Phys. Rev. A*, **39**(6), 3112–3119.

Malkin, A. J., Cheung, J. & McPherson, A. (1993). *J. Cryst. Growth*, **126**, 545–554.

Malkin, A. J. & McPherson, A. (1993*a*). *J. Cryst. Growth* **126**, 555–564.

Malkin, A. J. & McPherson, A. (1993*b*). *J. Cryst. Growth*, **128**, 1232–1235.

Meakin, P. (1988). In *Phase Transitions and Critical Phenomena*, Vol. 12, edited by C. Domb & J. L. Lebowitz, pp. 335–489. New York: Academic Press.

Muschol, M. & Rosenberger, F. (1995). *J. Chem. Phys.* **103**(24), 10424–10432.

Niimura, M., Minezaki, Y., Ataka, M. & Katsura, T. (1995). *J. Cryst. Growth*. **154**, 136–144.

Northrup, S. H. & Erickson, H. P. (1992). *Proc. Natl Acad. Sci. USA*, **89**, 3338–3342.

Provencher, S. W. (1982*a*). *Comp. Phys. Comm.* **27**, 213–227.

Provencher, S. W. (1982*b*). *Comp. Phys. Comm.* **27**, 229–232.

Pusey, P. N. & Tough, R. J. A. (1985). In *Dynamic Light Scattering*, edited by R. Pecora, pp. 85–171. New York: Plenum Press.

Riès-Kautt, M. M. & Ducruix, A. F. (1989). *J. Biol. Chem.* **263**, 745–748.

Riès-Kautt, M. M., Ducruix, A. F. & Dorsselaer, A. V. (1994). *Acta Cryst.* D**50**, 366–369.

Schaefer, D. W., Bunker, B.C. & Wilcoxon, J. P. (1989). *Proc. R. Soc. London Ser. A*, **423**, 35–53.

Schmitz, S. K. (1990). An *Introduction to Dynamic Light Scattering by Macromolecules*. New York: Academic Press.

Sibille, L. & Pusey, M. L. (1994). *Acta Cryst.* D**50**, 396–397.

Smoluchowski, M. v. (1916*a*). *Phys. Z.* **17**, 585–599.
Smoluchowski, M. v. (1916*b*). *Phys. Z.* **17**, 557–585.
Smoluchowski, M. v. (1917). *Z. Phys. Chem.* **92**, 129–168.
Sonntag, H. & Strenge, K. (1987). *Coagulation Kinetics and Structure Formation*. Berlin: VEB Deutscher Verlag der Wissenschaften.
Soumpasis, D. M. & Georgalis, Y. (1997). *Biophys. J.* In the press.
Taratuta, V. G., Holschbach, A., Thurston, G. M., Blankschtein, D. & Benedek, G. B. (1990). *J. Phys. Chem.* **94**, 2140–2144.
Thomson, J. A., Schurtenberger, P., Thurston, G. M. & Benedek, G. B. (1987). *Proc. Natl Acad. Sci. USA*, **84**, 7079–7083.
Umbach, P., Georgalis, Y. & Saenger, W. (1997). *J. Am. Chem. Soc.* Submitted.
Vicsek, T. (1989). *Fractal Growth Phenomena*. Singapore: World Scientific.
Wagner, C. (1961). *Z. Elektrochem.* **65**(7/8), 581–591.
Wills, P. R. & Georgalis, Y. (1981). *J. Chem. Phys.* **85**, 3978–3984.